Journal of Power Sources 196 (2011) 1371–1377

Contents lists available at ScienceDirect

Journal of Power Sources

journal homepage: www.elsevier.com/locate/jpowsour

The influence of the nitrogen-ion flux on structure and ionic conductivity of vapor deposited lithium phosphorus oxynitride films

Yoon Gu Kim*, H.N.G. Wadley

Department of Materials Science and Engineering, School of Engineering and Applied Science, University of Virginia, 395 McCormick Road, Charlottesville, VA 22904, USA

ARTICLE INFO

Article history:
Received 20 July 2010
Received in revised form 31 August 2010
Accepted 31 August 2010
Available online 8 September 2010

Keywords:
Lithium phosphorus oxynitride (Lipon)
Directed vapor deposition (DVD)
Hollow cathode plasma

ABSTRACT

Thin films of lithium phosphorus oxynitride (Lipon) have been grown using a plasma-assisted, directed vapor deposition (PA-DVD) technique. In this approach, a high voltage electron beam is used to vaporize a Li_3PO_4 source and a supersonic, nitrogen-doped, helium gas jet then transport the vapor towards a substrate. A hollow cathode technique was then used to create an argon plasma just above the substrate. This sufficiently ionized the nitrogen in the gas jet to allow its incorporation into the Li_3PO_4 film reactively forming lithium phosphorus oxynitride. Increasing the nitrogen flux in the gas jet also increased the deposition rate from 113 to 178 nm min^{-1} for the deposition conditions used here, significantly reduced the pore volume fraction in the films and increased the N/P ratio from 0 to 0.75 as the gas jet nitrogen flux was increased from zero to 4.3×10^{18} molecules cm^{-2} s^{-1}. Using substrate rotation, pore and columnar-free dense Lipon films could be grown by this method. The Li-ion conductivity increased from 3.7×10^{-9} to 5.2×10^{-7} S cm^{-1} as the nitrogen concentration was increased from zero to 2.1×10^{18} molecules cm^{-2} s^{-1} and was correlated with an increase in the film's Li/P ratio. An optimum nitrogen flux has been identified. As the nitrogen flux was increased above this value, the Lipon films suffered lithium loss and partial crystallization, resulting in a decrease in their Li-ion conductivity.

© 2010 Elsevier B.V. All rights reserved.

1. Introduction

Thin-film batteries are widely used as power sources in micro-electro-mechanical systems (MEMS) devices, smart cards, and in some implantable medical devices because of their small size [1,2]. Rechargeable thin-film Li/Li-ion batteries appear good candidates for these applications because they have a high-energy storage density compared to other many secondary battery chemistries [3]. Rechargeable thin-film Li/Li-ion batteries consist of a Li anode, a lithiated electrolyte and a lithium transition metal oxide cathode multi-layer structure sandwiched between a pair of metallic current collectors [4,5]. Radio frequency (RF)-magnetron sputtering approaches are usually used to synthesize the cathode and electrolyte layers and a thermal evaporation method employed to deposit the low melting temperature (~180 °C) lithium anode [5].

During a charge/discharge cycle, the thin-film electrolyte must permit the high mobility transport of lithium ions between the anode and cathode while blocking the conduction of electrons [6]. This requires the deposition of films of an appropriate (lithium rich) chemistry and structure that has a high lithium ion mobility and is free of through thickness defects (such columnar pores or cracks) that provide electron discharge pathways when a voltage is applied between the electrodes [7]. It is also essential that the decomposition potential of the thin-film electrolytes is higher than the target voltage of the battery system and that the ionic conductivity be as high as possible in order to minimize internal voltage drop losses [6].

Lithium phosphorus oxynitride (Lipon) electrolytes with a dense, but high mobility amorphous structure have attracted significant interest for thin-film battery applications [8]. Thin films of the electrolyte synthesized by RF-magnetron sputtering approaches [8–10] do not decompose when a 5.5 V potential is applied across them [8,9]. They also have an acceptable Li-ion conductivity (10^{-6} to 10^{-7} S cm^{-1} range) in the amorphous state [11] and very low electron conductivity (less than ~10^{-14} S cm^{-1}). Rechargeable thin-film lithium batteries that employ Lipon film electrolytes have also been shown to exhibit a high "cycleablity" (over 10,000 charge/discharge cycles) [12].

Unfortunately, the deposition of Lipon films by the RF-magnetron sputtering approach is slow (<2 nm min^{-1}). This arises because it is usually necessary to use a low plasma power (in the 12–40 W range) and a low pressure (20 mTorr) Ar–N_2 or pure N_2 working gas environment. Several alternative deposition approaches are being investigated for Lipon film deposition including pulsed laser deposition (PLD) [13], ion beam assisted deposition (IBAD) [14] and electron-beam (EB) evaporation [15]. However, they all suffer to a greater or less extent from very rough film surface morphologies, high film stresses, or similarly low deposition rates.

* Corresponding author. Tel.: +1 434 982 5035; fax: +1 434 982 5677.
E-mail address: ygk4x@virginia.edu (Y.G. Kim).

0378-7753/$ – see front matter © 2010 Elsevier B.V. All rights reserved.
doi:10.1016/j.jpowsour.2010.08.115

Recently, a plasma-assisted directed vapor deposition (PA-DVD) technique has been explored for the synthesis of Lipon films [16]. In this approach, a high power electron beam is used for high rate evaporation of lithium phosphate from a source positioned in the throat of an annular, gas jet forming nozzle. A supersonic nitrogen-doped helium gas jet is formed at the nozzle exit by maintaining a large pressure difference up and downstream of the nozzle opening. This jet entrains the vapor and transports it to a substrate with high deposition efficiency [17]. A hollow cathode plasma technique can be used to increase the reactivity of nitrogen in the gas jet and reactively deposit lithium phosphorus oxynitride films. This approach has been shown to enable the deposition of Lipon films at up to 45 times the deposition rate of the RF-magnetron sputtering approach. The initial study showed that the molecular assembly processes at the film growth surface were effected by the hollow cathode plasma forming current and this enabled manipulation of the Li-ion conductivity and pore content of the films [16]. The study identified a strong effect of the plasma current upon the conductivity, morphology and composition of the films, and identified the existence of an optimum set of plasma conditions for electrolyte deposition.

Here, we explore the effects of varying the concentration of the nitrogen in a nitrogen-doped helium gas jet used to reactively synthesize Lipon films by the PA-DVD approach. We find that the nitrogen concentration significantly affected the deposition rates of the films as well as their surface morphology, pore distribution, nitrogen concentration, and Li-ion conductivity. An optimum activated nitrogen flux is found that maximized the lithium ion mobility and Li/P ratio of Lipon films. Columnar-free dense Lipon films are then achieved even when using substrate rotation.

2. Experimental methods

2.1. Plasma-assisted directed vapor deposition

The plasma-assisted directed vapor deposition (PA-DVD) approach utilizes an electron-beam evaporation process to create a Li_3PO_4 evaporant, Fig. 1. Details of the process can be found in Refs. [17,18]. The Li_3PO_4 vapor is entrained in a supersonic nitrogen-doped helium gas jet formed by gas expansion through an annular nozzle whose inner and outer diameters are 2 and 3 cm respectively. The initially annular supersonic gas jet rapidly transports vapor atoms created at its core to a substrate that was positioned here approximately 22.0 cm from the source. This significantly increased source material utilization efficiency and the deposition rate. Nitrogen was added to the helium gas jet to facilitate reactive deposition of lithium phosphorus oxynitride films. For this to be achieved, the nitrogen was forced to pass through a plasma where it suffered partial electronic excitation, dissociation and ionization [19].

In the PA-DVD approach, a hollow cathode plasma technique has been utilized to activate the nitrogen and enhance its gas phase reaction rate with the lithium phosphate vapor. It also enables manipulation of the molecular assembly processes on the growth surface (thereby controlling porosity and the columnar growth mode) [20,21]. Here, a hollow cathode current of 60 A was used to create an argon plasma near the substrate and we investigated the effect of changing the $He:N_2$ ratio of the gas jet on film composition, structure and properties.

2.2. Deposition conditions

For the experiments conducted here, a 1.3 cm diameter cold pressed Li_3PO_4 source rod (Plasmaterials, Inc., CA, USA) was used for evaporation. A stable Li_3PO_4 vapor plume was created using an electron-beam power of 160 W. The evaporation rate was estimated by weighing the Li_3PO_4 source material before and after a timed evaporation run. For the incident electron-beam power density used here, the Li_3PO_4 evaporation rate was 2.05×10^{-4} g s^{-1} for all the experiments. The circular area over which the Li_3PO_4 vapor deposition occurred (at a source to substrate distance of 22.0 cm) was approximately 104.0 cm^2. If the source evaporation rate is divided by the formula mass of Li_3PO_4 ($\sim$115.8 g mol^{-1}) and the circular area, then the average incident Li_3PO_4 molecular flux was approximately 1.02×10^{16} molecules cm^{-2} s^{-1} for the source–substrate position used here. The Lipon films were grown using a nitrogen volume fraction in the helium gas jet that varied from 0.0 to 0.2. The total $He + N_2$ supersonic gas jet flux was held constant at $\sim 2.14 \times 10^{19}$ molecules cm^{-2} s^{-1}. The molecular nitrogen flux component in the jet therefore varied from 0 to 4.3×10^{18} molecules cm^{-2} s^{-1}.

Prior to each growth experiment, the deposition chamber was evacuated to a base pressure of 1.35×10^{-2} Torr. During the deposition process, this rose to 9.0–9.75 $\times 10^{-2}$ Torr. When the nitrogen fraction in the supersonic helium gas jet was increased, the density of the nitrogen-doped helium gas increased in the compartment under the nozzle, which resulted in an increase in the upstream pressure (P_u). This increased the P_d/P_u ratio from 3.8 to 4.4. The Lipon films were all grown at a substrate temperature of $\sim 180 \pm 20$ °C. One of the substrates was rotated at 5 rpm to if changing the inclination of the substrate during vapor deposition could eliminate void formation during growth of the films.

When a hollow cathode source is heated, its emitted thermionic electrons can be accelerated forming a low-voltage electron beam (LVEB). A previous study indicated that the use of a hollow cathode electron beam with an energy in the range of 5–15 eV is sufficient to ionize both the molecules of an evaporant and the nitrogen and so enhance their reactivity [16,20]. For the experiments conducted here, the hollow cathode utilized an argon working gas (with a flow rate of 0.1 slm) to form the initial plasma, Fig. 1. The plasma forming gas jet and coaxial LVEB were perpendicular to the nitrogen-doped gas jet forming a plasma just below the substrate. A substrate bias of −20 V was applied so that only positive ions were attracted towards the substrate. The substrate ion current density, J_s, was roughly estimated from the substrate ion current. It should be noted that numerous ionized species contributed to the ion current. As shown in Fig. 2, the substrate ion current density increased linearly from 3.9×10^{-4} to 5.4×10^{-4} A cm^{-2} as the nitrogen flux in the gas jet was increased. This corresponded to an ion flux (ions cm^{-2} s^{-1}) indicated in the right axis of Fig. 2.

2.3. Film characterization

The Lipon films were characterized using Scanning Electron Microscopy (SEM), X-ray diffraction (XRD), X-ray Photoelectron Spectroscopy (XPS), Inductively Coupled Plasma Optical Emission Spectroscopy (ICP-OES), and Electrochemical Impedance Spectroscopy (EIS). Details can be found in the previous study [16]. Scanning Electron Microscopy (SEM) was used to determine the deposition rates of Lipon films and then the deposition rates of all the films (by dividing the Lipon film thickness by the film deposition time).

3. Results and discussion

3.1. Film deposition rate

The deposition rate was gradually increased from 113 to 178 nm min^{-1} as nitrogen was added to the gas jet, Table 1. During the plasma-assisted deposition process, the direction of vapor transport was geometrically perpendicular to that of the argon

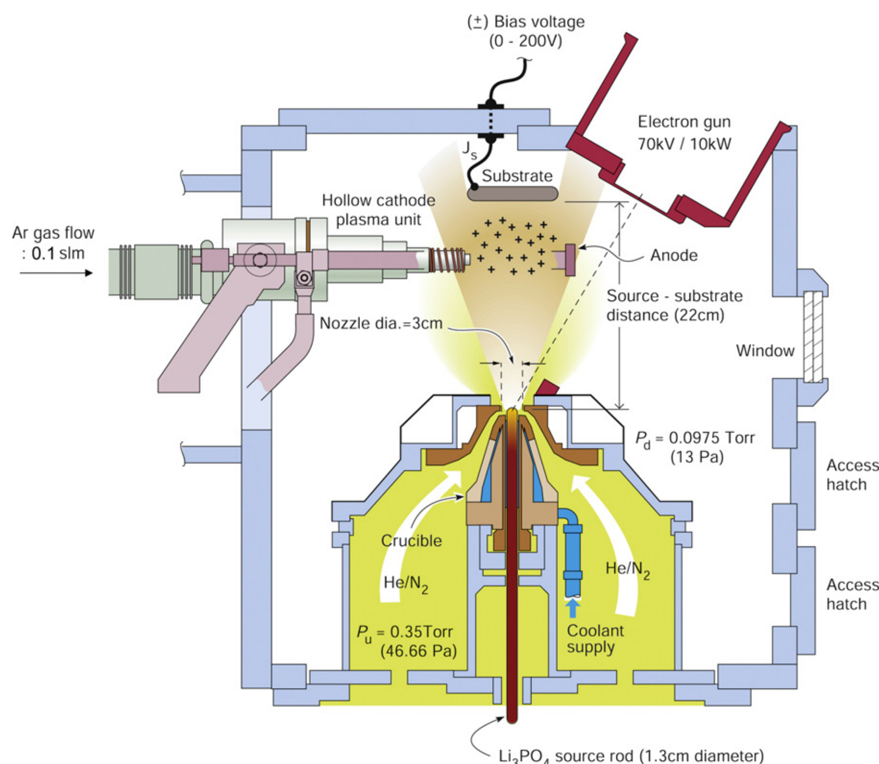

Fig. 1. The plasma-assisted, directed vapor deposition (PA-DVD) used to synthesize Lipon films. During a film deposition process, an electron beam was used to evaporate Li_3PO_4 source and the vapor was entrained in a rarefied supersonic He gas jet that was doped with varying concentration of N_2. The gas jet was then made to pass through a hollow cathode activated plasma created by a low-voltage electron discharge. The cathode to anode potential difference was around 40 V or less. The pressure upstream of the nozzle (P_u) and that downstream (P_d) controlled the gas jet speed.

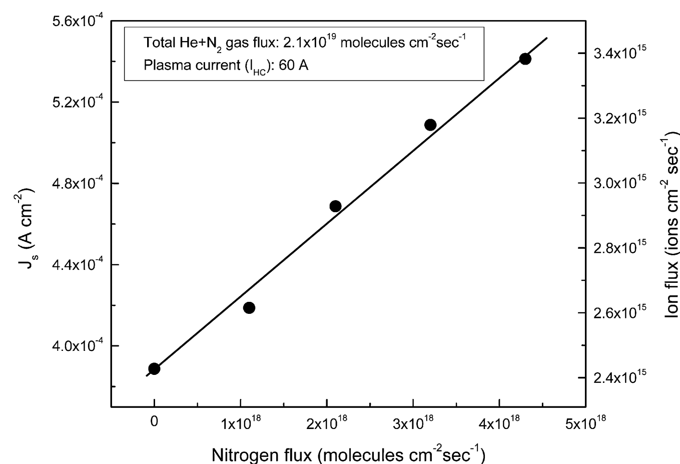

Fig. 2. Substrate plasma current density (J_s) and ion flux as a function of the nitrogen flux transported by the gas jet. An argon plasma current of 60 A was used here and the combined He + N_2 gas flux was held constant at the total 2.1×10^{19} molecules cm^{-2} s^{-1}.

plasma jet created by the hollow cathode source. This depositional geometry was not optimal resulting in deflection of light atoms away from the substrate and a decreased deposition rate of Lipon films [16]. However, as the nitrogen flux in the vapor transport jet was increased, lateral deflection of the light vapor molecules by the argon plasma jet was reduced and the deposition rate then increased. The highest deposition rate was over 50 times that reported for the RF-magnetron sputtering approach (~2 nm min^{-1}).

3.2. Film morphology

When Li_3PO_4 films were deposited without plasma assistance, their surface contained intercolumnar porosity, and the cross-section of the films contained many pores, and some traversed the entire film's thickness [16]. When the plasma was activated with a plasma current (I_{HC}) of 60A, nitrogen was incorporated in the Li_3PO_4 and lithium phosphorus oxynitride (Lipon) films were formed. Fig. 3(a) and (b) shows that the growth surface had spiral morphologies when the nitrogen flux was in the 1.1–2.1×10^{18} molecules cm^{-2} s^{-1} range. However, these spiral morphologies disappeared as the nitrogen flux was increased to 4.3×10^{18} molecules cm^{-2} s^{-1} and more energetic atomic assembly conditions were achieved on the film surface, Fig. 3(c). While none of the Lipon films deposited with a flux greater than 1.1×10^{18} molecules cm^{-2} s^{-1} contained surface breaking cracks.

As shown in Fig. 3(a)–(c), the cross-sections of the Lipon films changed from a porous columnar to a dense columnar structure as the nitrogen flux increased. For a nitrogen flux of

Table 1
Deposition conditions and deposition rates of Lipon films prepared by the total He + N_2 gas flow rate of 5.0 slm. Chamber vacuum pressure was 1.35×10^{-2} Torr. Note that P_d is the downstream pressure, P_u is the upstream pressure, and source-plasma distance was 12 cm. For the Lipon film growth, the plasma current of 60 A was used.

Nitrogen flow rate (slm)	Nitrogen flux (molecules cm^{-2} s^{-1})	Pressure ratio (P_d/P_u)	Deposition time (min)	Film thickness (μm)	Deposition rate (nm min^{-1})
0.25	1.1×10^{18}	3.8	30	3.4	113
0.5	2.1×10^{18}	4.2		3.8	128
1.0	4.3×10^{18}	4.4		5.3	178

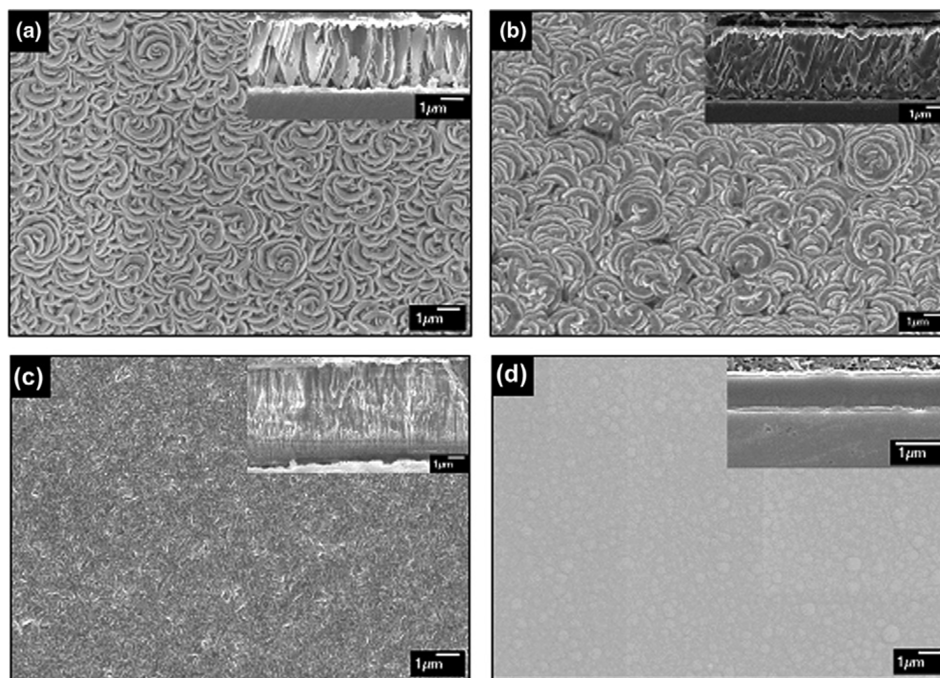

Fig. 3. Surface and cross-sectional morphologies of the Lipon films synthesized using various nitrogen fluxes in the gas jet: here, (a) 1.1×10^{18} molecules cm^{-2} s^{-1}, (b) 2.1×10^{18} molecules cm^{-2} s^{-1}, (c) 4.3×10^{18} molecules cm^{-2} s^{-1} (d) 2.1×10^{18} molecules cm^{-2} s^{-1} and substrate rotation of 5 rpm. Insets in Fig. 3(a)–(d) show cross-sections of Lipon films deposited using a plasma assistance of 60 A.

1.1×10^{18} molecules cm^{-2} s^{-1}, large pores were located at inter-columnar boundaries. Examination of Fig. 3(a) shows that for low nitrogen fluxes, the films growth columns were initiated from widely separated nuclei. The diameter of the growth columns increased with film thickness and had impinged upon one another after about 1 μm of growth. Increasing the nitrogen flux and therefore the ion current greatly reduced the pore fraction in these Lipon films. However, even films grown with a nitrogen of 4.3×10^{18} molecules cm^{-2} s^{-1} retained a columnar structure that can facilitates electrolyte breakdown during repeated charge and discharge [7].

When the substrate was rotated in combination with a high nitrogen flux the columnar mode of film growth could be eliminated and smooth, dense, void and crack free films could be formed. Fig. 3(d) shows an example of a film grown with a rotation rate of 5 rpm. As shown in the inset of Fig. 3(d), the substrate rotation completely removed columnar structures caused by geometrical vapor shadow effects. The reasons for this change in growth mode may result from reduced geometrical vapor shadowing during film deposition. The formation columnar-free dense Lipon structures are a critical in the fabrication of rechargeable thin-film batteries because these structures inhibit electrode batteries.

3.3. Film composition

Previous studies have shown that use of plasma assistance enables incorporation of nitrogen into the Li_3PO_4 structure [16]. The electron energies generated by the hollow cathode were in the range of 5–15 eV, which is sufficient to dissociate nitrogen bonds (~9.8 eV) and ionize nitrogen (~14.53 eV) [22]. This activation clearly led to nitrogen incorporation in the Li_3PO_4 films deposited here.

As the nitrogen flux was increased, the N/P ratio was found to linearly increase to a value of 0.75 at a flux of 4.3×10^{18} molecules cm^{-2} s^{-1}, Fig. 4. The Li/P ratio also initially increased with increasing nitrogen flux but then reached a maximum at a flux of 2.1×10^{18} molecules cm^{-2} s^{-1}, Fig. 5. The initial rise is thought to be a consequence of an increase in the upstream gas jet forming pressure P_u by the addition of nitrogen. This increased the P_u/P_d ratio and thus the jet speed as nitrogen was added to the supersonic helium gas jet. Increases to the jet speed then increases entrainment of the Li_3PO_4 vapor atoms in the jet plume and the rate of deposition [17]. This effect was eventually compensated by the increase in activated nitrogen flux in the gas jet. This led to an increase in the N/P ratio and a reduction of the Li/P ratio in the Lipon films [16,23,24].

3.4. Film structure

Amorphous films are generally preferred as thin-film electrolytes because they have a more isotropic and higher ionic conductivity than equivalent composition crystalline films [6,25]. They

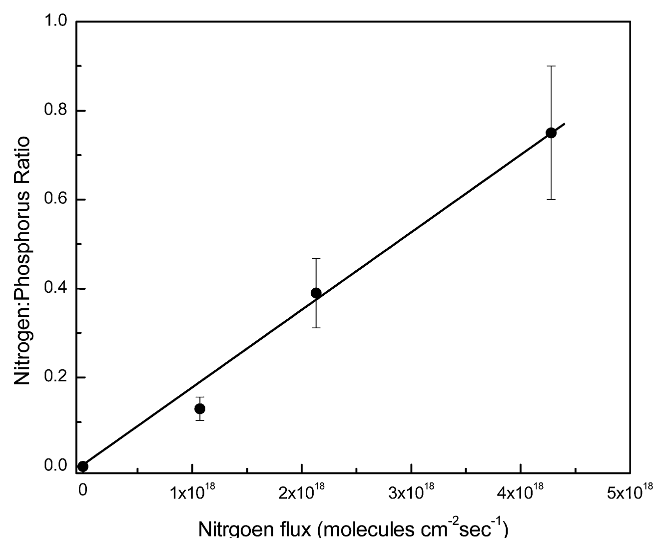

Fig. 4. N/P ratio of Lipon films as a function of the gas jet. The N/P ratio was obtained by XPS. The error bars represent ±10% of the N/P ratio.

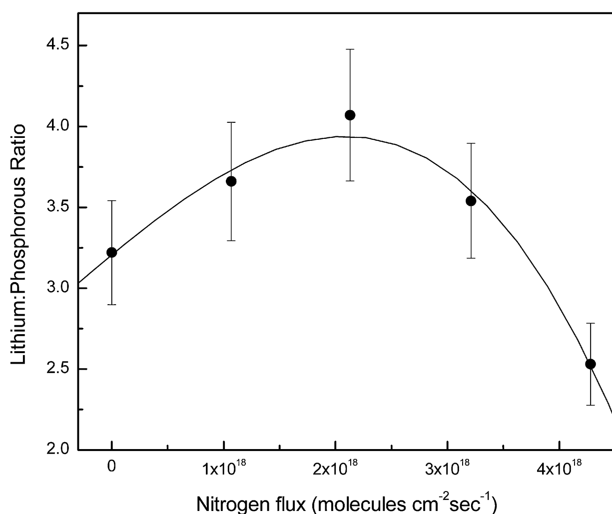

Fig. 5. Li/P ratio of Lipon films as a function of the nitrogen flux in the helium gas jet. The Li/P ratio was determined by ICP-OES. The error bars are ±5% of the Li/P ratio.

are also preferred because they do not require a post-deposition annealing (crystallization) step, which can be problematic for multi-layer structures with different coefficients of thermal expansion. The structures of the films deposited here were investigated by X-ray diffraction and XRD patterns for each film as shown in Fig. 6. The XRD data for most films contained no sharp diffraction peaks. They are therefore indicative of an amorphous structure. However, as the nitrogen flux was increased to 4.3×10^{18} molecules $cm^{-2}\,s^{-1}$, weak crystalline peaks began to be observed in addition to the diffuse scattering associated with the amorphous phase. The positions of these weak peaks are consistent with the presence of the γ-Li_3PO_4 crystal phase [26,27]. They suggest the existence of local crystallized phases that may have formed by increased growth surface mobility associated with a high incident energetic ion flux.

When nitrogen substitutes for oxygen in Li_3PO_4, the charge on the phosphorus ions changes [28]. Consequently, there should be a shift in binding energy (BE), since this is approximately proportional to the charge of atoms [28,29]. The binding energy change, $\Delta(BE_i)$, can be written:

$$\Delta(BE_i) = k \cdot \Delta q_i \quad (1)$$

where Δq_i is the change in the charge on the ith ion and k is a proportionality constant [29]. XPS technique can be used to determine the nitrogen coordination state in an as-deposited film and enables an investigation of the inter-atomic binding. The carbon binding energy, C_{1s} = 285 eV, were used as a reference peak position to correct the P_{2p} XPS peak positions shifted by the XPS charging effects of samples.

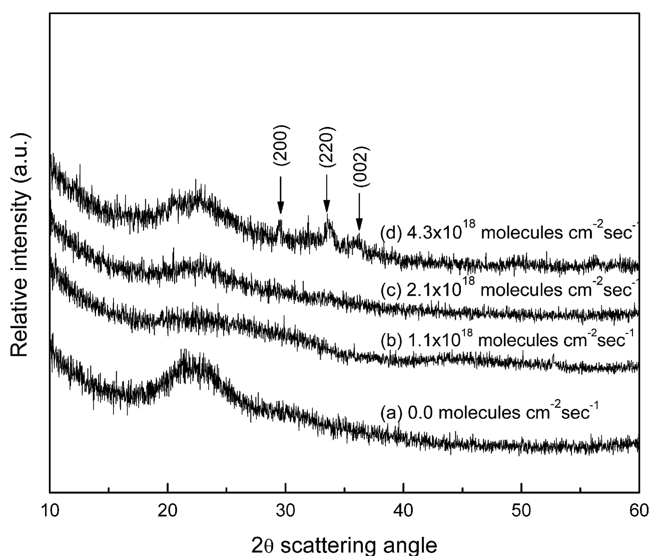

Fig. 6. X-ray diffraction patterns of Lipon films synthesized using gas jets with the different nitrogen fluxes. The curve marked (a) used a pure He jet and no plasma assistance. The other curves show the effect of increasing the N_2 flux within the gas jet from 1.1 to 4.3×10^{18} molecules $cm^{-2}\,s^{-1}$ at I_{HC} = 60 A. The XRD patterns indicate that Lipon films grown using low N_2 flux were amorphous. However, the film grown using the higher N_2 flux contained regions of crystalline material.

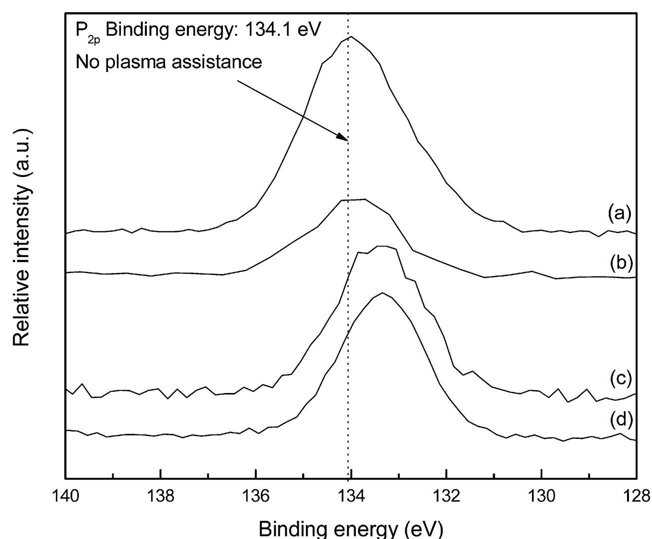

Fig. 7. XPS P_{2p} peak shift for a lithium phosphate films (a) and Lipon films synthesized using gas jets containing a nitrogen flux of 1.1×10^{18} (b), 2.1×10^{18} (c), and 4.3×10^{18} molecules $cm^{-2}\,s^{-1}$ (d). The vertical line shows the phosphorus binding energy of Li_3PO_4 film (134.1 eV). Increasing the nitrogen flux in the helium gas jet lowers the phosphorus binding energy of Lipon films.

Brow et al. indicated that the P_{2p} XPS peaks of $NaPO_xN_y$ type compounds were shifted down in energy from 134.8 to 133.9 eV upon incorporation of nitrogen [30]. Our previous studies with Lipon also indicated that the XPS P_{2p} peaks were shifted from 134.1 down to 132.8 eV upon incorporation of nitrogen [16]. This reduction in P_{2p} binding energy arises because P–O bonds are gradually replaced by P–N bonds. Fig. 7 shows that when nitrogen was added to helium gas jet, the XPS P_{2p} peaks of Lipon films were shifted from 134.1 to 133.3 eV. This result is consistent with nitrogen replacing oxygen in the Li_3PO_4 film and with the increase of the N/P ratio in the films, Fig. 4.

3.5. Li-ion conductivity of Lipon films

Using stainless steel/Lipon/Au test cells, the Li-ion conductivities of the films were measured by electrochemical impedance spectroscopy (EIS) [16,31]. The complex impedance $Z(\omega)$ was measured over the 1–10^5 Hz frequency (ω) range with 0.1 logarithmic increments. As shown in Fig. 8, the real and imaginary components of the impedance are plotted and fitted by a circuit model, Fig. 8(a). When the $Z(\omega)$ graphs form a depressed semicircular arc, they are usually fitted by an empirical Cole–Cole equation with the form [31]:

$$Z(\omega) = R_{hf} + \frac{R_o - R_{hf}}{1 + (j\omega\tau)^n}, \quad (2)$$

where R_o = resistance at low-frequency (Ω), R_{hf} = resistance at high-frequency (Ω), $\tau = (R_o - R_{hf}) \times C$, in which C = capacitance (F), and $0 \le n \le 1$. By fitting the impedance results obtained here to

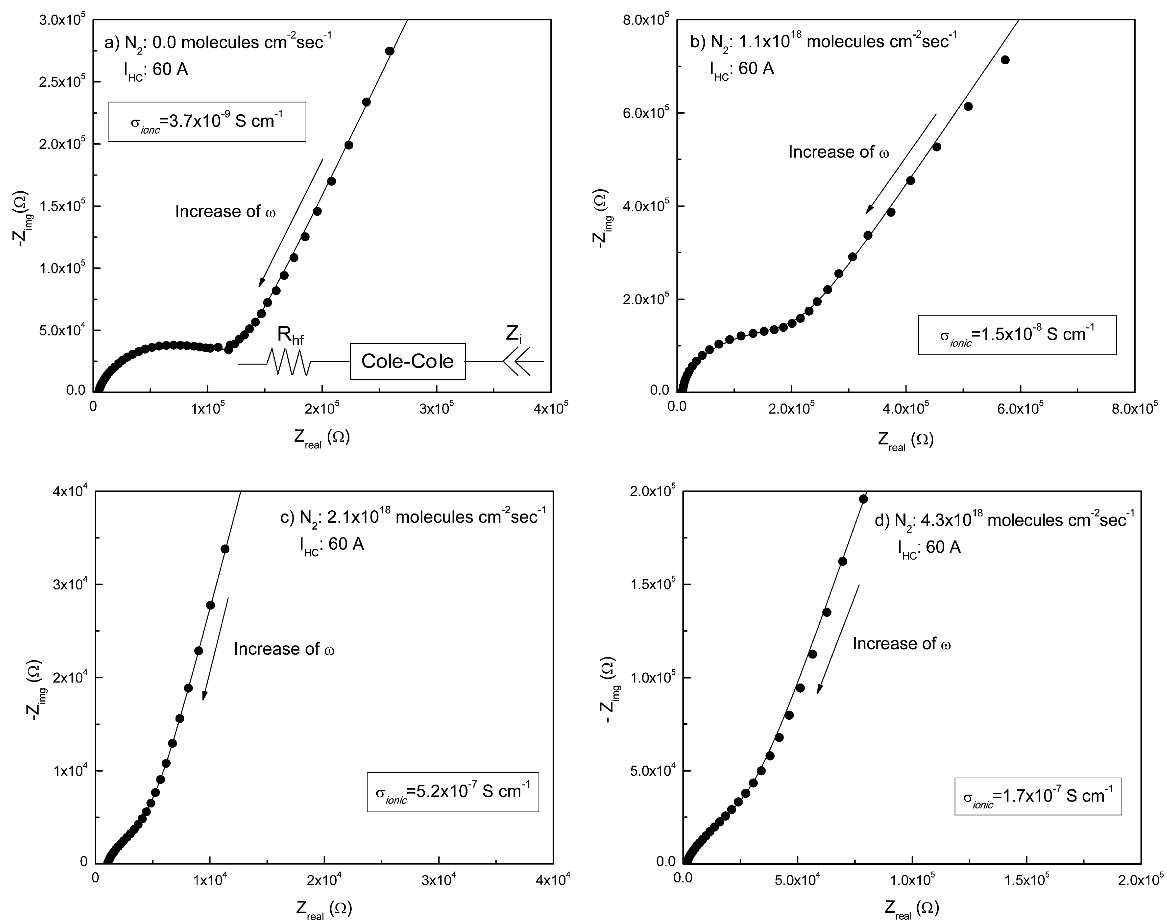

Fig. 8. Electrochemical impedance spectra for (a) lithium phosphate film and (b–d) Lipon films synthesized using gas jets containing nitrogen dimmer up to 4.3×10^{18} molecules $cm^{-2}\,s^{-1}$. The impedance was measured between 1 and 10^5 Hz. The dots correspond to experimental data while the solid lines are a best fit to the electrochemical circuit model shown in the inset of (a) [16,31]. The deduced Li-ion conductivity for each film is also shown.

the Cole–Cole equation, we could deduce the film resistance, $R_{el} = R_o - R_{hf}$. Because the interface between the Au layer and Lipon film was neither a perfect ion-blocking electrode nor ideally smooth, EIS spectra do not exhibit a pure capacitive response at low-frequency (the EIS spectra do not meet the real impedance axis at a 90°) [6]. In view of this, an interfacial impedance, $Z_i = C_i \cdot (j \cdot \omega)^{-n}$, was introduced into the Cole analysis to characterize the low-frequency response. The Lipon resistance was then used to find the conductivity, σ_{ionic}, using the relation:

$$\sigma_{ionic} = \frac{d}{R_{el} \times A}, \quad (3)$$

where d is the thickness of the Lipon film, A is the area of the test cell, and R_{el} is the resistance of Lipon films deduced by fitting the data to the Cole–Cole equation. This data is summarized in Table 2.

Table 2
Fitting parameters used to calculate Li-ion conductivities of the Lipon films prepared on a stainless steel substrate. Subscript letters represent as follows: hf = high-frequency, el = electrolyte (Lipon), g = geometrical, and i = interface between electrolyte and metallic electrode. A circuit model is given in Fig. 8(a).

Nitrogen flux (molecules $cm^{-2}\,s^{-1}$)	0.0	1.1×10^{18}	2.1×10^{18}	4.3×10^{18}
R_{hf} (Ω)	3000	2000	900	1300
n_{el}	0.7	0.92	0.76	0.81
R_{el} (Ω)	1.17×10^5	1.58×10^5	3.7×10^3	2.47×10^4
C_g (F)	2.3×10^{-9}	1.8×10^{-10}	3.8×10^{-9}	1.6×10^{-9}
n_i	0.7	0.68	0.87	0.8
C_i (F)	8.0×10^{-7}	1.5×10^{-8}	2.5×10^{-8}	2.3×10^{-8}

The Lipon films were sandwiched by an area (A) of 0.049 cm^2. A detail description of this analysis can be found in other references [16,31].

The Li-ion conductivities of the films are summarized in Table 3. The films were all prepared with plasma assistance since those grown without plasma assistance suffered from electrical shorts due to their porous and highly cracked film structure [16]. The Li_3PO_4 film made in this way had a Li-ion conductivity of $3.7 \times 10^{-9}\,S\,cm^{-1}$. When nitrogen was incorporated in the films, Li-ion conductivities increased into 10^{-7} to $10^{-8}\,S\,cm^{-1}$ range. The highest Li-ion conductivities in Table 3 are comparable to those reported for Lipon films synthesized by the e-beam evaporation approach [32]. As mentioned in the earlier Section 3.4, the amorphous Li_3PO_4 and Lipon materials proven by the XRD patterns have much higher conductivity values than crystalline materials that are in the 10^{-13} to $10^{-18}\,S\,cm^{-1}$ range [11]. This result indicates that the amorphous Li_3PO_4 and Lipon materials may have more free volumes to transport Li ions than the crystalline materials [25].

Table 3
Li-ion conductivities of the Lipon films. The Li-ion conductivities (σ_{ionic}) of the films were obtained by Eq. (3). The area (A) of electrodes was 0.049 cm^2.

Nitrogen flux (molecules $cm^{-2}\,s^{-1}$)	Thickness (μm)	σ_{ionic} ($S\,cm^{-1}$)
0.0	0.2	3.7×10^{-9}
1.1×10^{18}	1.1	1.5×10^{-8}
2.1×10^{18}	1.0	5.2×10^{-7}
4.3×10^{18}	2.0	1.7×10^{-7}

The data in Table 3 indicate that the Li-ion conductivity increased monotonically from 3.7×10^{-9} to 5.2×10^{-7} S cm^{-1} as the nitrogen concentration in the gas jet increased. This can be understood by recalling the relationships between structural changes and nitrogen incorporation. Because the atomic radii of nitrogen atoms (1.32 Å) are larger than those of oxygen atoms (1.24 Å), incorporation of nitrogen atoms in Li_3PO_4 causes a structural distortion. Wang et al. investigated the structure of bulk polycrystalline Lipon by X-ray and neutron diffraction [11]. They found that nitrogen incorporation in Li_3PO_4 increased the average Li–O bond distance. Because a binding energy between lithium and oxygen is inversely proportional to the Li–O bond distance, this increase of average Li–O bond length reduces the Li–O binding energy and enhances lithium ion mobility in the Li_3PO_4 structure. Furthermore, since the lithium ion is located within a LiO_4 tetrahedron, it should pass through one of the triangular face of the tetrahedron for diffusion to occur. Because the increase in average Li–O bond length increases the area of a triangular face in the LiO_4 tetrahedron, lithium ions can more easily diffuse through them as the nitrogen content increases. Thus, as nitrogen atoms are incorporated in the Li_3PO_4 system, the Li-ion conductivities are expected to increase.

However, the data in Table 3 indicate that when Lipon films were synthesized using very high nitrogen fluxes, the Li-ion conductivity began to decrease (to 1.7×10^{-7} S cm^{-1}, Table 3). This appears to be result of the loss of lithium in the films and the partial crystallization of the Lipon films (see Figs. 5 and 6). This observation appears to be consistent with the previous study where increases of the N/P ratio decreased the Li/P ratio and reduced Li-ion conductivity [16].

Previous studies indicated that rechargeable thin-film lithium batteries had an acceptable charge–discharge cycle, provided the Li-ion conductivity of Lipon films is higher than 1.2×10^{-8} S cm^{-1} [33]. When the Li-ion conductivity dropped to 7.2×10^{-9} S cm^{-1}, serious voltage losses were observed. These results above indicate that a Li-ion conductivity in the high 10^{-7} S cm^{-1} range obtained using the PA-DVD deposition approach may be suitable for rechargeable thin-film lithium battery applications.

4. Summary

The effects varying the activated nitrogen flux incident upon the surface of Lipon films grown from lithium phosphate sources have been explored using a PA-DVD deposition approach. As the nitrogen flux and nitrogen content of the films was increased, the atomic structure of Lipon films changed from an amorphous structure to a partially crystallized amorphous structure. This was accompanied by a change in surface morphology from one covered by spiral rings to a spiral-free smooth surface. The cross-sections also changed from a porous columnar structure to a structure consisting of dense, tightly packed columns. These changes appear to be a consequence of an increase in the reaction rate of high-energy nitrogen ions with the evaporated lithium phosphate on the substrate surface. Substrate rotation enabled synthesis of columnar-free, dense Lipon films. As the nitrogen flux incident on the growth was increased, the N/P ratio of Lipon films increased up to 0.75. The XPS P_{2p} binding energy shifts indicated that the nitrogen ions replaced oxygen atoms in the Li_3PO_4 structure. As the nitrogen flux was increased to 2.1×10^{18} molecules cm^{-2} s^{-1}, the Li-ion conductivities of the films increased from 3.7×10^{-9} S cm^{-1} to reach a maximum of 5.2×10^{-7} S cm^{-1}. This increased Li-ion conductivity was attributed to the increase of nitrogen concentration in the films with the nitrogen flux. Further increases of the nitrogen flux decreased the Li-ion conductivity because of lithium losses and partial crystallizations in the films. The Li-ion conductivities of the Lipon films were comparable to those reported by e-beam evaporation approaches. However, the use of a supersonic nitrogen-doped helium gas jet concentrated the vapor resulting in a deposition rate that was over 50 times that reported for other deposition approaches.

References

[1] S.D. Jones, J.R. Akridge, J. Power Sources 54 (1995) 63.
[2] J.B. Bates, N.J. Dudney, B. Neudecker, A. Ueda, C.D. Evans, Solid State Ionics 135 (2000) 33.
[3] J.M. Tarascon, M. Armand, Nature 414 (2001) 359.
[4] J.B. Bates, N.J. Dudney, D.C. Lubben, G.R. Gruzalski, B.S. Kwak, X. Yu, R.A. Zuhr, J. Power Sources 54 (1995) 58.
[5] J.B. Bates, N.J. Dudney, B.J. Neudecker, B. Wang, Presented at Thin-film lithium batteries, Gordon and Breach, 2000.
[6] P.G. Bruce, Solid State Electrochemistry, Cambridge University Press, 1997.
[7] S.O. Kasap, Principles of Electrical Engineering Materials and Devices, McGraw-Hill, 1997.
[8] J.B. Bates, N.J. Dudney, G.R. Gruzalski, R.A. Zuhr, A. Choudhury, C.F. Luck, J.D. Robertson, Solid State Ionics 53–56 (1992) 647.
[9] X. Yu, J.B. Bates, J.G.E. Jellison, F.X. Hart, J. Electrochem. Soc. 144 (1997) 524.
[10] Y. Hamon, A. Douard, F. Sabary, C. Marcel, P. Vinatier, B. Pecquenard, A. Levasseur, Solid State Ionics 177 (2006) 257.
[11] B. Wang, B.C. Chakoumakos, B.C. Sales, B.S. Kwak, J.B. Bates, J. Solid State Chem. 115 (1995) 313.
[12] B. Wang, J.B. Bates, F.X. Hart, B.C. Sales, R.A. Zuhr, J.D. Robertson, J. Electrochem. Soc. 143 (1996) 3203.
[13] S. Zhao, Z. Fu, Q. Qin, Thin Solid Films 415 (2002) 108.
[14] F. Vereda, R.B. Goldner, T.E. Haas, P. Zerigian, Electrochem. Solid-State Lett. 5 (2002) A239.
[15] Z.W. Fu, W.Y. Liu, C.L. Li, Q.Z. Qin, Y. Yao, F. Lu, Appl. Phys. Lett. 83 (2003) 5008.
[16] Y.G. Kim, H.N.G. Wadley, J. Vac. Sci. Technol. A 26 (2008) 174.
[17] J.F. Groves, Ph.D. Dissertation, University of Virginia, 1998.
[18] J.F. Groves, Y. Marciano, D.D. Hass, G. Mattausch, H. Morgner, H.N.G. Wadley, Presented at Society of Vacuum Coaters, 44th Annual Technical Conference Proceedings, Philadelphia, 2001.
[19] N. Newman, J. Cryst. Growth 178 (1997) 102.
[20] H. Morgner, M. Neumann, S. Straach, M. Krug, Surf. Coat. Technol. 108–109 (1998) 513.
[21] S. Schiller, C. Metzner, O. Zywitzki, Surf. Coat. Technol. 125 (2000) 240.
[22] L. Pauling, General Chemistry, Dover Publications, 1988.
[23] S. Veprek, S. Iqbal, J. Brunner, M. Scharli, Philos. Mag. 43 (1981) 527.
[24] L. Boukbir, R. Marchand, Rev. Chim. Min. 23 (1986) 343.
[25] T. Minami, N. Machida, Mater. Sci. Eng. B 13 (1992) 203.
[26] R.K. Osterheld, J. Inorg. Nucl. Chem. 30 (1968) 3173.
[27] T.Y. Tien, F.A. Hummel, J. Am. Ceram. Soc. 44 (1961) 206.
[28] U. Gelius, Phys. Scr. 9 (1974) 133.
[29] R.K. Brow, C.G. Pantano, J. Am. Ceram. Soc. 69 (1986) 314.
[30] R.K. Brow, M.R. Reidmeyer, D.E. Day, J. Non-Cryst. Solids 99 (1988) 178.
[31] E. Barsoukov, J.R. Macdonald, Impedance Spectroscopy, Wiley-Interscience, 2005.
[32] W.Y. Liu, Z.W. Fu, C.L. Li, Q.Z. Qin, Electrochem. Solid-State Lett. 7 (2004) J36.
[33] H. Park, S. Nam, Y. Lim, K. Choi, K. Lee, G. Park, S.R. Lee, H. Kim, S. Cho, J. Electroceram. 17 (2006) 1023.